J Fluoresc (2014) 24:523–531
DOI 10.1007/s10895-013-1321-8

ORIGINAL PAPER

Turn-off Fluorescence Chemosensor for Iron with Bis(2-aminoethyl)-2-(9-fluorenyl)malonamide Functionlized SBA-15

Marzieh Yadavi · Alireza Badiei

Received: 13 July 2013 / Accepted: 7 November 2013 / Published online: 3 December 2013

Abstract An bis(2-aminoethyl)-2-(9-fluorenyl)malonamide as fluorophore ligand was immobilized onto mesoporous silica type SBA-15 via post synthesis grafting. The obtained material was characterized by small and wide angle X-ray diffraction, N_2 adsorption–desorption, Fourier transform infrared spectroscopy, Raman spectroscopy and thermogravimetric analysis that indicate the successful immobilization of the ligand on the surface of mesoporous silica. The sensing ability of the obtained material was studied by addition of the cations Fe^{3+}, Mg^{2+}, Cr^{3+}, Co^{2+}, Ni^{2+}, Cu^{2+}, Hg^{2+} and Zn^{2+} to water suspensions of the assayed solid. Of all the cations tested addition of Fe^{3+} ion to a suspension of this material resulted in the largest decrease in the fluorescence intensity. Turn-off photoluminescence of this material was remarkably observed for iron ions in comparing of the other cations. A good linearity between the fluorescence intensity of this material and the concentration of Fe^{3+} ion is constructed, which enables it as a fluorescence chemosensor for detecting the Fe^{3+} ion with a suitable detection limit of 1.35×10^{-5}. It can be introduced as a novel fluorescent sensor in aqueous solution for a lot of practical applications in chemical, environmental and biological systems.

Keywords Mesoporous silica · SBA-15 · Fluorene · Fluorescence · Fe^{3+} ions chemosensor

M. Yadavi · A. Badiei (✉)
School of Chemistry, College of Science, University of Tehran, Tehran, P. O. Box: 14155-6455, Iran
e-mail: abadiei@khayam.ut.ac.ir

M. Yadavi
e-mail: marziyadavi@khayam.ut.ac.ir

A. Badiei
Nanobiomedicine Centra of Excellence, Nanoscience and Nanotechnology Research Centra, University of Tehran, Tehran, Iran

Introduction

Synthesizing chemosensors based on ion-induced fluorescence changes for specific metals detection are predominantly attractive because of their high selectivity, sensitivity, simplicity and low detection limit of fluorescence recognition methods [1–3]. In the middle of it all, fluorescence 'turn-off' sensors for detection of metal ions of biological importance still remain a challenging aspect [4, 5]. Hence, much attention has been paid to the design of 'turn-off' fluorescence sensors. Among the metal ions, Fe^{3+} is of particular interest owing to its established role in biological and industrial areas that is indispensable for most organisms, and both its deficiency and overload can induce various disorders [6]. Furthermore improved method for the detection and sensing of Fe^{3+} ions with high selectivity is of current interest in the sensor research field. Only a few examples of sensor showing fluorescence changes upon Fe^{3+} complexation have been reported [7, 8]. However, the majority of these reports were just based on organic molecules as fluorescent chemosensors [7–9]. For some practical applications the attachment of the fluorophore to a solid support has advantages like the possibility of recovering the materials for their repetitive use and operation at the nanoscale level [10, 11].

Organic-functionalized mesoporous silica type SBA-15 can provide synergistic properties of organic and inorganic components, such as flexible surface chemistry to functionalization, well-defined ordered structure, available surface area, structural stability and the large pore diameter allows grafting of bulky organic moieties have attracted much attention in recent years [12–18]. Sensor selectivity towards transition metal ions can be modified by changing the structural features of the mesoporous silica, we are currently designing and testing new sensors consisted of fluorenyl and other chelating units [19, 20]. These materials have selectivity and sensitivity to detect metal ions. Some have been reported to recognize Zn^{2+} [21], Cu^{2+} [22], Pb^{2+} [23] and Hg^{2+} [24] in

aqueous media. However, material has been no reported to recognize iron ions that operate at the nanoscale level in aqueous media [19, 20]. Herein we report the synthesis of a functionlized mesoporous silica based material bis(2-aminoethyl)-2-(9-fluorenyl)malonamide that functions as a Fe^{3+} sensor at aqueous solution. In view of high chemical stability and fluorescent emission of fluorenyl, first we linked it as fluorophore to a dioxotetramine receptor then, to the inner surface of cholor functionalized mesoporous support SBA-15 (SBA-Cl) and obtained a new fluorescent Fe^{3+} sensor in aqueous solution. To the best of our knowledge, this is the first example of a fluorescent sensor based on bis(2-aminoethyl)-2-(9-fluorenyl)malonamide functionlized SBA-15 that allows the selective detection of Fe^{3+} in aqueous media. Moreover, in the presence of Fe^{3+}, this sensor shows highly selective and sensitive recognition toward Fe^{3+} in over a wide range of tested cations including Mg^{2+}, Cr^{3+}, Co^{2+}, Ni^{2+}, Cu^{2+}, Hg^{2+} and Zn^{2+} without fluorescence intensity change. Compared with other reported fluorescent chemosensors for Fe^{3+} ions, this system showed the highest selectivity toward Fe^{3+} ions in aqueous solution.

Experimental

Materials and Instruments

Poly (ethylene glycol)-block-poly (propylene glycol)-block-poly (ethylene glycol) ($EO_{20}PO_{70}EO_{20}$) (P123, MW=5800) was obtained from Aldrich. Fluorene, bromine, carbon tetrachloride, diethyl ether, tetraethylorthosilicate (TEOS), 3-chlorpropyltriethoxysilane, sodium carbonate, diethyl malonate, ethylendiamine and hydrochloric acid were obtained from Merck. Iron (III) nitrate, magnesium nitrate, cupper (II) nitrate, cobalt (II) nitrate, nickel (II) nitrate, chromium (III) nitrate, mercury (II) nitrate and zinc nitrate were of analytical grade. Toluene and DMF was dried according to the standard purification methods [25]. Nitrogen physisorption isotherms were obtained on a BELSORP mini-II at liquid nitrogen temperature (77 K). Surface area was measured using the Brunauer-Emmett-Teller (BET) method, pore size distributions were calculated from the nitrogen isotherms by Barrett-Joyner-Halenda (BJH) method. Small and wide angle x-ray scattering (SAXS) patterns were recorded with a model Hecus S3-MICROpix SAXS diffractometer with a one-dimensional PSD detector using Cu Kα radation (50KV, 1 mA) at wave length 1.542 Å. FT-IR spectra were recorded a 4000–600 cm^{-1} region on Equinox 55 spectrometer. Raman spectra were obtained on SENTERRA spectrometer. Thermogravimetric analysis (TGA) was performed on a TA Q50 instrument. The scans were performed between 20 °C and 800 °C at 10 °C/min. Emission spectra were recorded on Perkin-Elmer LS50 model luminescence spectrometer. Fluorescence measurements were done in a 1 cm quartz cuvette containing a magnetic-stirred solution of compounds in aqueous solvent (0.1 g L^{-1}). Calcinations were carried out in a box furnace Gofa in the presence of flowing air. Melting points were determined by the capillary method on electro thermal 9100 apparatus.

Synthesis SBA-15

SBA-15 material was prepared according to literature procedures [19, 20, 26, 27].

Synthesis Chloro-functionalized of SBA-15

0.85 g of 3-chlorpropyltriethoxysilane was added drop wise to 1.25 g of vacuum dried mesoporous silica SBA-15 dispersed in 60 ml of dry toluene under an inert atmosphere (Ar) in a flask fitted with a reflux condenser and a magnetic stirrer. Then the mixture was refluxed at 95 °C for 24 h and the final product was filtered, washed with toluene and dried at room temperature.

Synthesis 9-bromofluorene

9-bromofluorene was prepared by literature methods [19, 20].

Synthesis Diethyl 2 - (9 -fluorenyl)malonate (Flem)

The diethyl 2 -(9 -fluorenyl)malonate material was synthesized in accordance with the procedure reporte by Luo et al. [28]. To a solution of diethyl malonate (4.28 g, 0.027 mol) in anhydrous DMF (5 ml) were added Na_2CO_3 (2.83 g, 0.027 mol) and a solution of 9-bromofluorene (6.56 g, 0.027 mol) in DMF (20 ml). The resulting mixture was stirred at 70 °C for 24 h and poured into 250 ml ice water. The suspension formed was extracted with three 25 ml portions of diethyl ether. The organic layer was dried over Na_2SO_4 and the solvent was removed by rotary evaporation to give a yellow solid. After recrystallization from ethanol, yellow needle crystals were obtained (Fig. 1.); m.p. 69–72 °C, ν_{max}/cm^{-1} 2977 (ν_{CH}), 1727 (ν_{CO}), 1447 and 1367 (ν_{CH}), 735 ($\nu_{C\text{-}C}$).

Synthesis Bis(2-aminoethyl)-2-(9-fluorenyl)malonamide (Flen)

The bis(2-aminoethyl)-2-(9-fluorenyl)malonamide material was synthesized in accordance with the procedure reported by Luo et al. [28]. The mixture of the diethyl 2 -(9 -fluorenyl)malonate (6.28 g, 0.001 mol) and freshly distilled ethylenediamine (5 ml) was stirred at 35 °C for 72 h. Excess ethylenediamine was distilled off under reduced pressure. After cooling, the yellow residue was treated and washed with diethyl ether (Fig. 1.). ν_{max}/cm^{-1} 3281 (ν_{OH}) 3057 and 2865 (ν_{CH}),1655 (ν_{CO}), 1538 (ν_{NH}), 744 ($\nu_{C\text{-}C}$).

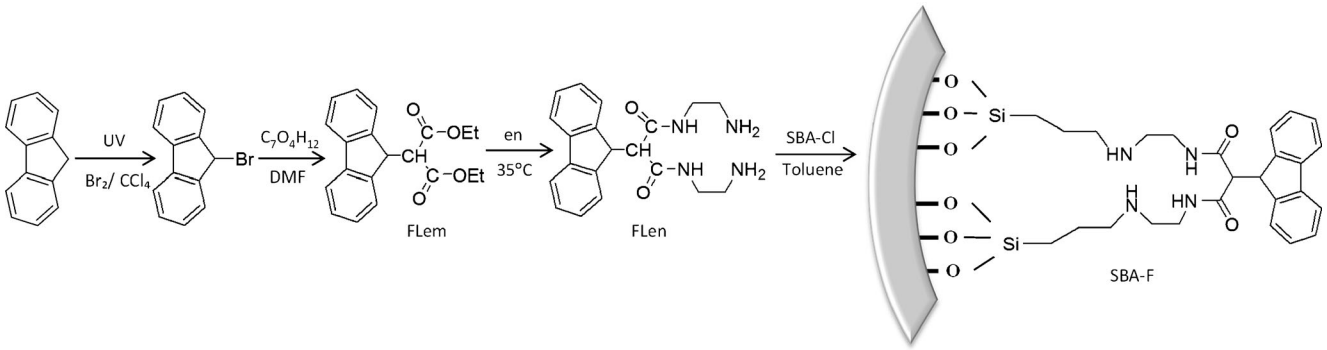

Fig. 1 Preparation of SBA-F

Synthesis Fluorene Functionalized SBA-15 (SBA-F)

0.1 g of SBA-Cl was placed in a vacuum for 30 min, then 20 mL of dry toluene was added and stirred for 15 min; bis(2-aminoethyl)-2-(9-fluorenyl)malonamide (0.1 g, 0.285 mmol) was added to the resulting mixture under an inert atmosphere and refluxed for 24 h. Next, it was allowed to cool at room temperature and the toluene was removed by filtration under vacuum and was dried at room temperature.

Results and Discussion

Small and Wide Angle X-ray Diffraction

Figure 2 shows the small and wide angle X-ray diffraction patterns of SBA-15 and the functionalized SBA-15 with chloropropyl groups and Flen. All samples have a single intensive reflection at 2θ angle at around 0.87° similar to the typical SBA-15 materials, that is a generally recognized characteristic of the long-range periodic [17]. For all the materials, two additional peaks related to the higher ordering (110) and (200) reflections can be also observed, which is associated with a two-dimensional hexagonal (p6mm) structure [17]. However, in the case of functionalized SBA-15 materials, the peak (100) intensity with a small peak shift decreases after immobilizations due to the difference in the scattering contrast of the pores and the walls, and to the irregular coverage of organic groups on the nanochannels. This observation indicates that the hexagonal structure of the SBA-15 is maintained without any pore wall collapse during the modifying of the surface. The larger wall thickness of the functionalized SBA-15 is consistent with grafting the organic groups onto the pore walls within the porous network (Table 1).

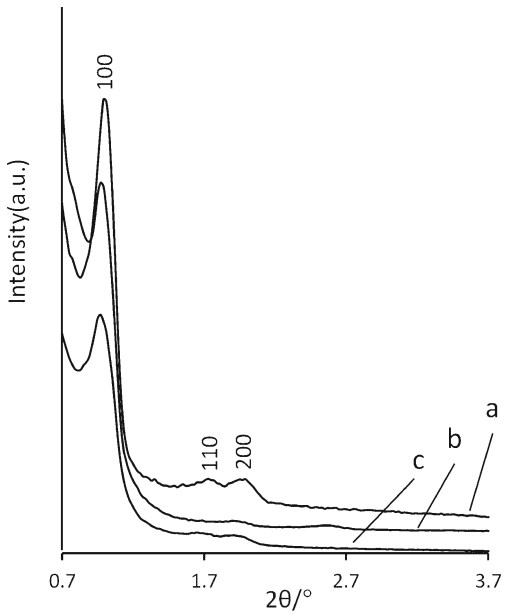

Fig. 2 Small angle XRD patterns **a**) SBA-15, **b**) SBA-Cl and **c**) SBA-F

N_2 Adsorption-Desorption

The textural properties of the samples were evaluated by the N_2 adsorption-desorption isotherms (Fig. 3). All materials exhibit a typical irreversible type IV nitrogen adsorption isotherm with an H1 hysteresis loop as defined by IUPAC [17]. There is a shift of the hysteresis position toward low relative pressures and a slight decreasing trend in overall N_2 adsorption volume as the loading of chloropropyl groups and FLen. This indicates some modification of the tubular channels of the parent SBA-15 silica material. The N_2 adsorption at low

Table 1 Texture properties of prepared compounds

Sample	D_{BJH} (nm)	S_{BET} (m^2 g^{-1})	V_{total} (cm^3 g^{-1})	w_t^a (nm)	d_{100}(nm)
SBA-15	6.2	587	0.78	3.06	8.06
SBA-Cl	5.4	470	0.73	4.98	9.04
SBA-F	4.7	167	0.29	5.72	9.07

S_{BET} is the BET surface area; V is the total pore volume; D_{BJH} is the average pore diameter calculated using BJH method

[a] Wall thickness $= 2/\sqrt{3}d_{(100)}$−pore diameter

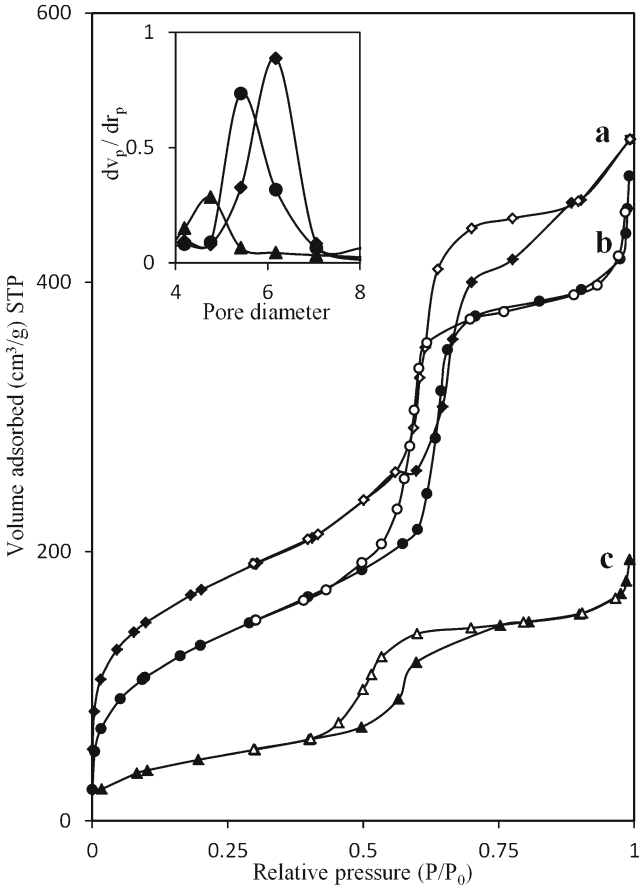

Fig. 3 N_2 adsorption-desorption isotherms of (**a**) SBA-15, (**b**) SBA-Cl, (**c**) SBA-F (Inset: BJH pore size distribution curves of SBA-15, SBA-Cl, SBA-F)

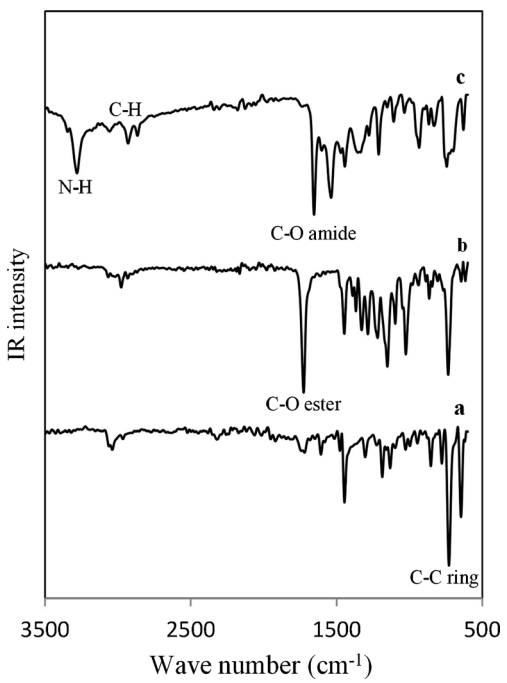

Fig. 4 FT-IR spectra of (**a**) 9-bromofluorene, (**b**) Flem, (**c**) Flen

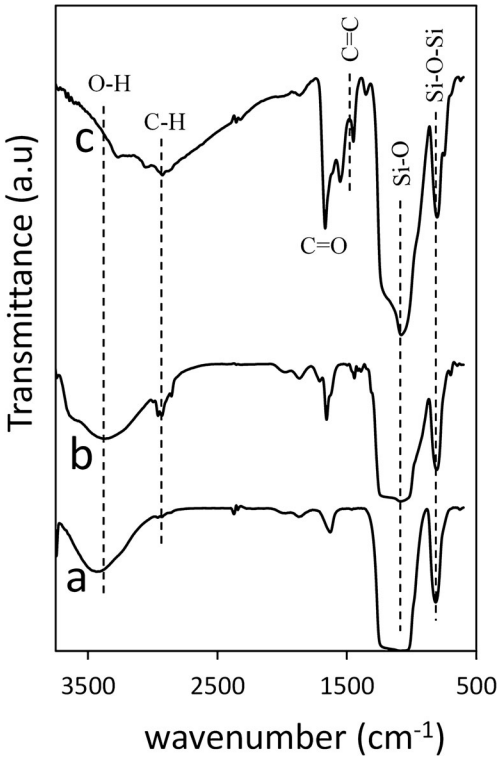

Fig. 5 FT-IR spectra of (**a**) SBA-15, (**b**) SBA-Cl, (**c**) SBA-F

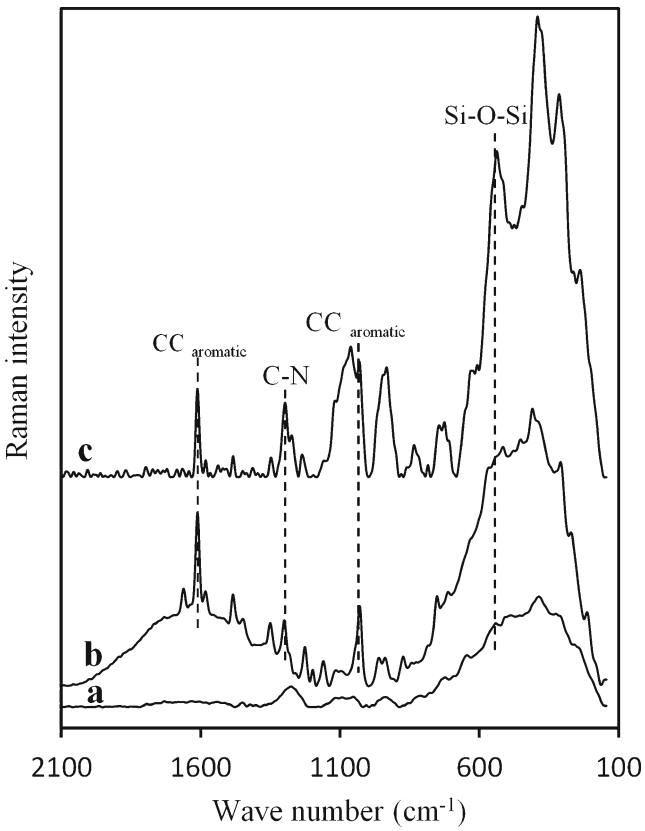

Fig. 6 Raman spectra of (**a**) SBA-15, (**b**) SBA-Cl, (**c**) SBA-F

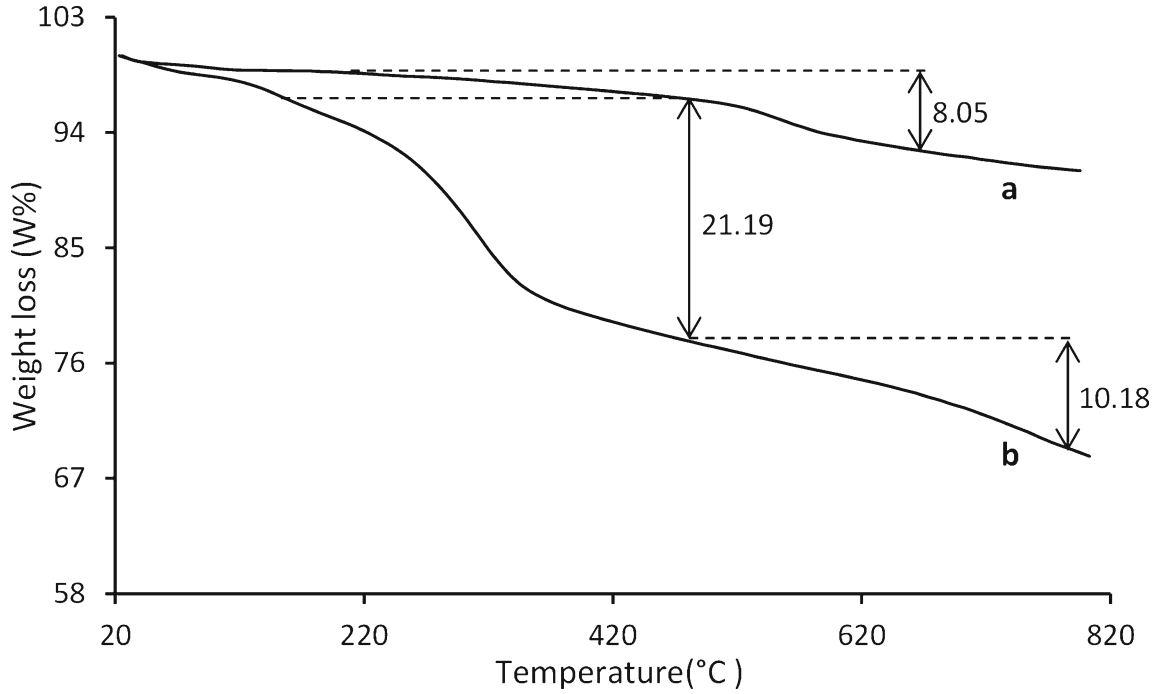

Fig. 7 TGA analysis of (**a**) SBA-Cl (**b**) SBA-F

relative pressures is accounted for by monolayer adsorption of N_2 on the pore walls, and does not essentially involve the presence of micropores. The sharp inflection in the P/P_0 range from 0.37 to 0.75 of the isotherm is characterized as capillary condensation within uniform mesopores, the position of which is clearly correlated to a diameter in the mesopore rang. The pore size distribution can be calculated from BJH method based on the desorption branch of the N_2 adsorption isotherm. As demonstrated in Fig. 3, a typical BJH plot from modified SBA-15 with chloropropyl groups and FLen a narrow pore size distribution are observed. The uniformity of the mesopores in this modified SBA-15 is comparable to the

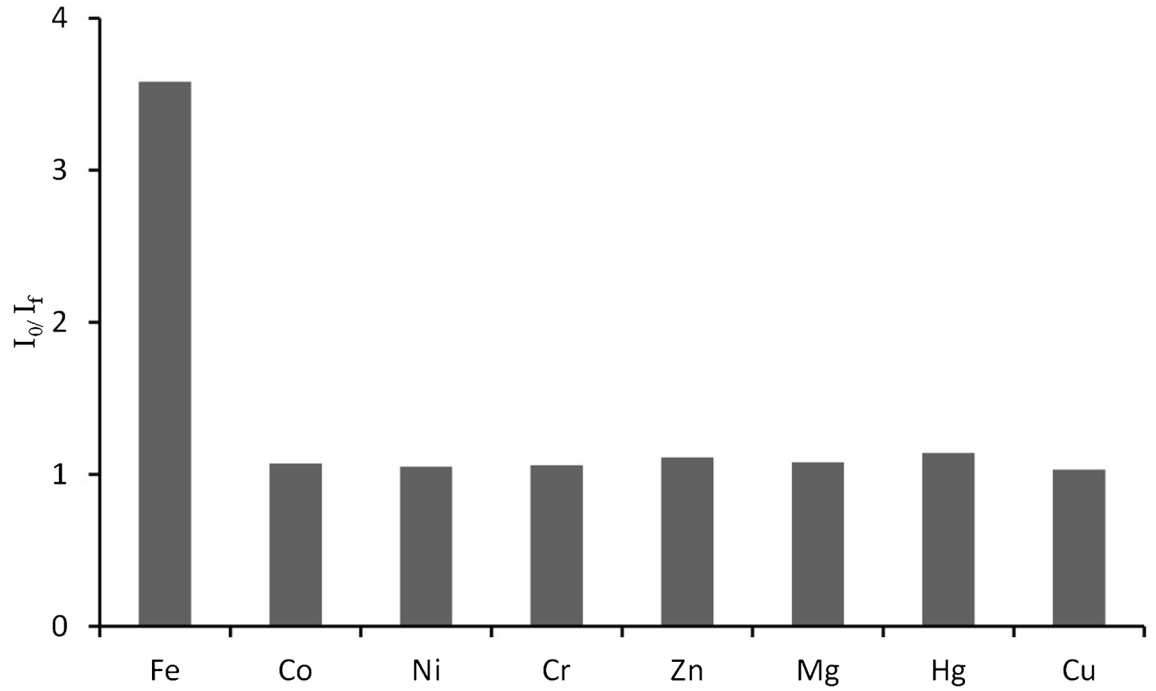

Fig. 8 Bar graphs of the fluorescence emission intensity for Fe^{3+}, Co^{2+}, Ni^{2+}, Cr^{3+}, Zn^{2+}, Mg^{2+}, Hg^{2+} and Cu^{2+} metal ions showing the metal ions selectivity profile of SBA-F (200 μg/2.0 mL) with a concentration of 0.16 mM for each metal ion. I_0 corresponds to emission of SBA-F without metal ions

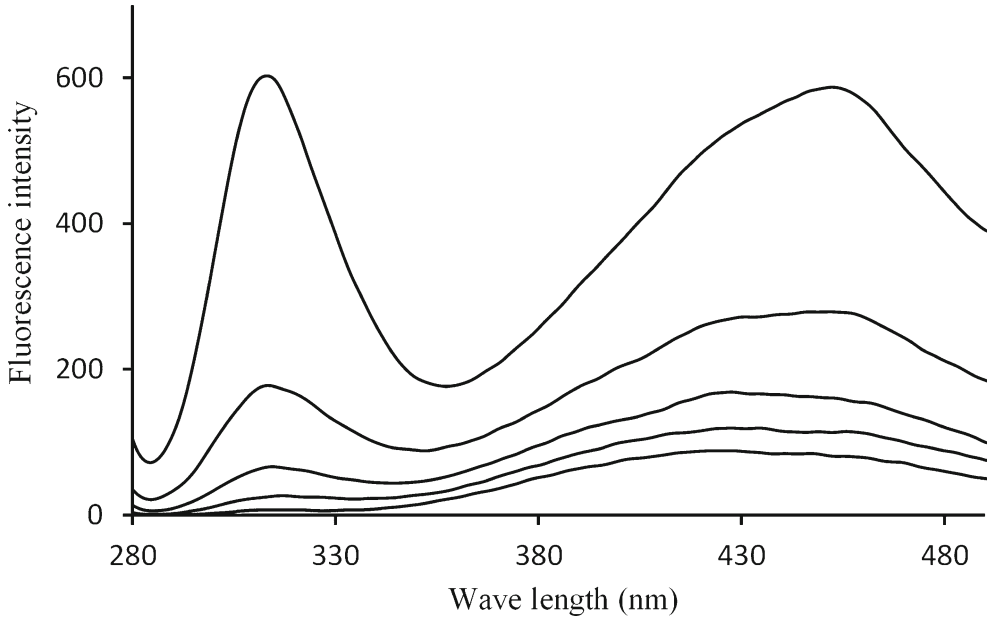

Fig. 9 Fluorescence emission spectra SBA-F (0.1 g.L^{-1}) in the presence of Fe^{3+} ions from 0.16 to 0.66 mM (λ_{ex}=260 nm)

SBA-15, indicating that the integrity of the original inorganic wall structure of the SBA-15, is retained. In comparison with SBA-15 decreasment in the pore diameter value by about 0.8 and 1.5 nm are observed for SBA-Cl and SBA-F, respectively. The textural parameters, specific surface areas (BET method), pore diameters (BJH method) and total pore volumes are given in Table 1, which shows a trend of decreasing in surface area, pore volume and pore diameter due functionalization inside the channels of SBA-15.

FT-IR Spectroscopy

The IR spectra of precursor compounds Flem and Flen exhibit two bands at about 740 and 725 cm^{-1} assigned to the skeleton stretching vibration of the aromatic ring that observe in the 9-bromofluorene (Fig. 4). In Flem, the band at 1725 cm^{-1} is the typical stretching frequency of the carbonyl in the ester. In Flen, the band at 1672 cm^{-1} is the typical stretching frequency of the carbonyl in the amide.

Figure 5 shows FT-IR spectra of SBA-15, SBA-Cl and SBA-F. In the FT-IR spectrum of the SBA-15 silica the band at 3434 cm^{-1} can be assigned to the stretching vibration of OH groups. The bands at 800 and 1086 cm^{-1} are attributed to Si-O-Si and Si-O stretching vibrations, respectively [29]. There is an abundance of silanol groups present in the parent SBA-15 silica in the surface of the mesoporous channels. After grafting chloropropyl on the surface of SBA-15, the intensity of the band at 3434 cm^{-1} is decreased. The band at 2930 cm^{-1} is assigned to C-H stretching vibrations of the methylene groups. These results indicated that the chloropropyl group was attached on the surface of SBA-15. SBA-F showed the band at 1670 cm^{-1} is the typical stretching frequency of the carbonyl in amid and the strong peak of 1450 cm^{-1} was observed which due to the C=C ring skeletal vibrations.

Raman Spectroscopy

Figure 6 shows the Raman spectra of SBA-15, SBA-Cl and SBA-F. The band at 2900 cm^{-1} is attributed to C-H stretching in the propyl chain in SBA-Cl and SBA-F. In the Raman spectra of SBA-F clearly the strong bands at 1610 and 1024 cm^{-1} are related to the C-C and C=C ring skeletal vibrations of FLen. The band at 1350 cm^{-1} is attributed to C-N vibrations that confirm FLen was attached on the surface of SBA-15.

TGA Analysis

TGA analysis was carried out to verify the grafted organic groups on the surface SBA-15. The TGA profiles samples are illustrated in Fig. 7. The weights loss at temperature of approximately 100 °C corresponded to desorption of physisorbed water, which is 0.7 % and 1.6 % for SBA-Cl and SBA-F, respectively [30]. The weight loss 8.1 % at 180–600 °C is mainly due to the decomposition of chloropropyl groups in SBA-Cl. The weights loss (21.19 % and 10.18 %)

Table 2 The charge densities and radius of metal ions

Element	Co^{+2}	Zn^{2+}	Mg^{2+}	Ni^{2+}	Cr^{3+}	Cu^{2+}	Hg^{2+}	Fe^{3+}
R	0.745	0.74	0.72	0.69	0.615	0.73	1.02	0.490
ρ	1.15	1.18	1.28	1.45	3.08	1.22	0.45	6.09

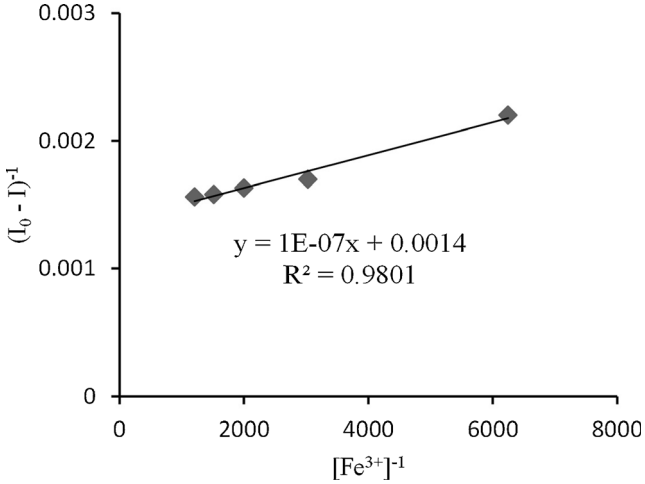

Fig. 10 Variation of $(I_0 - I)^{-1}$ of emission as a function of $[Fe^{3+}]^{-1}$ for SBA-F

between 200 and 800 °C are due to the decomposition of organic groups in SBA-F. A minor weights loss due to silanol condensation at high temperature was observed [31].

Fluorescence Study

The fluorescence emission spectra of SBA-F (200 μg/2.0 mL) in water exhibited one fluorescence emission at 310 nm and the else at 410 nm (λ_{ex}=260 nm) due to the fluorescent molecule fluorene grafted to the mesoporous silica. The second emission could be observed between 360 nm to 410 nm for fluorene that depends on the media [32]. This emission is attributed to a novel kind of twisted intermolecular charge transfer (TICT) conformer within the life time of the lowest excited singlet state [33]. With the addition of Fe^{3+}, the emission peak intensity decreased significantly. No obvious responses could be observed upon the addition of Mg^{2+}, Cr^{3+}, Co^{2+}, Ni^{2+}, Cu^{2+}, Hg^{2+} and Zn^{2+} (Fig. 8).

These observations indicated that SBA-F had a high sensitivity and excellent selectivity for Fe^{3+} in water. The results of fluorimetric titration indicate that fluorescence of fluorenyl was quenched by transfer of electron from metal center to photoexcited state of fluorenyl during coordination of Fe^{3+}. As shown in Fig. 9, a decrease of fluorescence intensity could be remarkably observed with an increasing Fe^{3+} concentration.

This high selectivity can be interpreted in terms of difference in charge densities of metal ions. It is well known that the charge density (ρ) of a metal ion is defined as the amount of electric charge/unit volume. It is one of the most important characterizations of the relative electrophilicity of a metal ion. The charge densities of metal ions were calculated according to the Eq. (1):

$$\rho = q/\left(4/3\pi r^3\right) \quad (1)$$

Where q is the formal charge and r denotes the Shannon ionic radius (Table 2) [34]. The calculated charge densities of the cations increase in the following order: Hg^{2+} (0.45)<Co^{2+} (1.15)<Zn^{2+} (1.18)<Cu^{2+} (1.22)<Mg^{2+} (1.28)<Ni^{2+} (1.45)< Cr^{3+} (3.08)<Fe^{3+} (6.09).

The results indicate that the charge density of Fe^{3+} ion is the biggest among all of the competition ions. Accordingly, the electrophilicity ability of Fe^{3+} ion is the strongest among these cations that can be used to interpret the capability of forming a coordination complex with an electron-rich ligand. Thus, the strong coordinate interaction between Fe^{3+} ions with the lone pair of the amine groups onto SBA-F significantly quench the fluorescence of fluorene because of the strong electrophilicity ability when it mixes with the other competition ions in the analytic solutions.

Figure 10 shows the plot of $(I_0 - I)^{-1}$ vs. $[Fe^{3+}]^{-1}$, where I_0 and I refer to the emission fluorescence intensity at 310 nm for SBA-F in the absence and presence of Fe^{3+} ions, respectively.

Generally, the mechanism of fluorescence quenching is divided into three types: dynamic quenching; static quenching; energy transfer [35]. Each of them is depicted through its special equation. A good linearity should be developed in the plot of $(I_0 - I)^{-1}$ vs. $[Fe^{3+}]^{-1}$ for the static

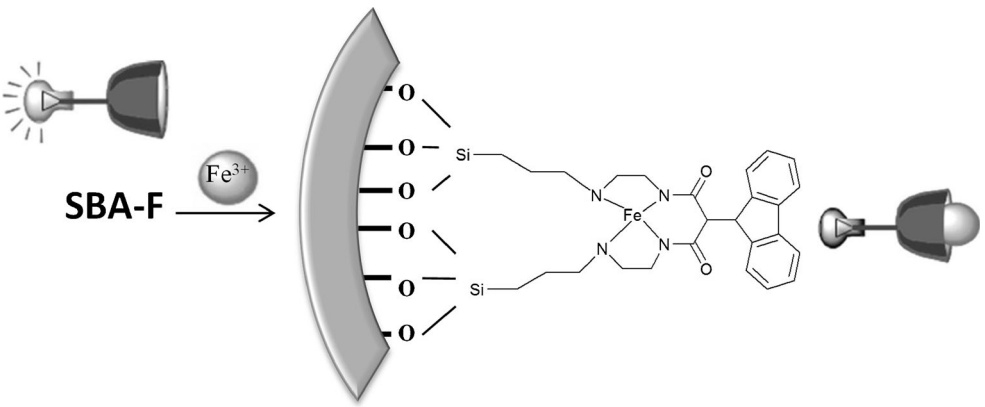

Fig. 11 Fe^{3+} binding with SBA-F

quenching mechanism according to the following Line weaver-Burk Eq. (2) [36]:

$$(I_0 - I)^{-1} = I_0^{-1} + K_D(I_0[Q])^{-1} \quad (2)$$

As seen in Fig. 10, a good linearity between $(I_0 - I)^{-1}$ and the reciprocal of the concentration of Fe^{3+} from 0.16 to 0.83 mM (linearly dependent coefficient R^2=0.98) is constructed. According to the above equation, the dissociation constant K_D can be obtained from the slope and intercept of the line and the corresponding association constant K ($1/K_D$) is 1.4×10^4. Also the detection limit of SBA-F for monitoring of Fe^{3+} are calculated according to Eq. (3), where DL is the minimal analytical signal that can be detected, S_D is the standard deviation of blank and m is the plot slope of fluorescence intensity vs. [Fe^{3+}].

$$DL = 3/S_D m \quad (3)$$

Therefore detection limit of SBA-F is 1.35×10^{-5}.

Considering that the result of fluorescence titration of SBA-F by Fe^{3+} is well-consistent with the Line weaver-Burk equation, we tentatively assign this quenching process as a static quenching mechanism that involves the interaction between the fluorescence molecule and the metal ions to form a nonfluorescent complex. This interaction often takes place in the ground state of the fluorescence molecule, and the quenching efficiency is governed by the formation constants and the concentration of metal ions [37]. Figure 11 shows the Fe^{3+} ions binding with SBA-F.

Conclusion

We have introduced a selective and sensitive method to detect aqueous iron ions based fluorene functionalized mesoporous silica. The FLen reacts with chloro-modified surfaces and is characterized with different techniques. Small and wide angle X-ray analysis showed that the mesoporous structure was preserved during process. N_2 adsorption-desorption isotherms display opening pores. Surface area and pore size decreased by attaching the Flen to the pore surface. FT-IR and Raman spectra demonstrated the incorporation of chloro functional groups and FLen on the surface of SBA-15. Also thermogravimetric analysis indicates the successful immobilization of organic groups on the surface of mesoporous silica. The sensing ability of SBA-F was studied by the cations Fe^{3+}, Mg^{2+}, Cr^{3+}, Co^{2+}, Ni^{2+}, Cu^{2+}, Hg^{2+} and Zn^{2+}. In response to iron ions, the system provided remarkable fluorescence intensity change. Moreover, compared with the reported sensors for Fe^{3+} ions, this is the first chemosensor based on bis(2-aminoethyl)-2-(9-fluorenyl)malonamide functionalized SBA-15 that can selectively detect iron ions in an aqueous environment. A good linearity between the fluorescence intensity of SBA-F and the concentration of Fe^{3+} ion is constructed, which enables this martial as a fluorescence chemosensor for detecting the Fe^{3+} ion with a suitable detection limit of 1.35×10^{-5}. We believe that the sensor can be promoted for a lot of practical applications in chemical, environmental and biological systems.

Acknowledgments The authors are grateful for the financial support from the University of Tehran.

References

1. Js K, Dt Q (2007) Calixarene-derived fluorescent probes. Chem Rev 107:3780–3799
2. Apd S, Hqn G, Gunnlaugsson T, Ajm H, Cp M, Jt R, Te R (1997) Signaling recognition events with fluorescent sensors and switches. Chem Rev 97:1515–1566
3. Hn K, Lee M, Hj K, Js K, Yoon J (2008) A new trend in rhodamine-based chemosensors: application of spirolactam ring-opening to sensing ions. Chem Soc Rev 37:1465–1472
4. Chen W, Tu X, Guo X (2009) Fluorescent gold nanoparticles-based fluorescence sensor for Cu^{2+} ions. Chem Commun 0:1736–1738
5. Yi C, Tian W, Song B, Zheng Y, Qi Z, Qi Q, Sun Y (2013) A new turn-off fluorescent chemosensor for iron(III) based on new diphenyl fluorenes with phosphonicacid. J Lumin 141:15–22
6. Ad C, Jr R (1994) Macromolecules 27:1975–1977
7. Sahoo S, Sharm D, Rk B, Crisponi G, Callan J (2012) Iron(III) selective molecular and supramolecular fluorescent probes. Chem Soc Rev 41:7195–7227
8. Zhang X, Chenga G, Zhang W, Shen G, Yu R (2007) A fluorescent chemical sensor for Fe^{3+} based on blocking of intramolecular proton transfer of a quinazolinone derivative. Talanta 71:171–177
9. Sui B, Kim B, Zhang Y, Frazer A, Belfield K (2013) Highly selective fluorescence turn-on sensor for fluoride detection. ACS Appli Mater Interfaces 5:2920–2923
10. Bl S, Moniotte N, Nivarlet N, Chen Lh F, Zy DJ, Li J (2011) Fl–DFO molecules@mesoporous silica materials: Highly sensitive and selective nanosensor for dosing with iron ions. J Colloid Inter Sci 358: 136–145
11. Jq W, Huang L, Xue M, Wang Y, Gao L, Zhu J, Zou Z (2008) Architecture of a hybrid mesoporous chemosensor for Fe^{3+} by covalent coupling bis-schiff base PMBA onto the CPTES-functionalized SBA-15. J Phys Chem C 112:5014–5022
12. Hoffmann F, Cornelius M, Morell J, Froba M (2006) Silica-based mesoporous organic–inorganic hybrid materials. Angew Chem 45: 3216–3251
13. Brunel D, Ac B, Galarneau A, Fajula F (2002) New trends in the design of supported catalysts on mesoporous silicas and their applications in fine chemicals. Catal Today 73:139–152
14. Vos Ded M, Bfs D, Pa J (2002) Ordered mesoporous and microporous molecular sieves functionalized with transition metal complexes as catalysts for selective organic transformations. Chem Rev 102: 3615–3640
15. Ap W, Me D (2002) Design and preparation of organic–inorganic hybrid catalysts. Chem Rev 102:3589–3614
16. Mcmorn P, Gj H (2004) Heterogeneous enantioselective catalysts: strategies for the immobilisation of homogeneous catalysts. Chem Soc Rev 33:108–122
17. Zhao D, Qs H, Jl F, Bf C, Gd S (1998) Nonionic triblock and star diblock copolymer and oligomeric surfactant syntheses of highly

ordered, hydrothermally stable, mesoporous silica structures. J Am Chem Soc 120:6024–6036
18. Ryoo R, Jun S (1997) Improvement of hydrothermal stability of MCM-41 using salt effects during the crystallization process. J Phys Chem B 101:317–320
19. Yadavi M, Badiei A, Mohammadi ziarani G (2013) A novel Fe^{3+} ions chemosensor by covalent coupling fluorene onto the mono, di- and tri-ammonium functionalized nanoporous silica type SBA-15. Appli Surf Sci 279:121–128
20. Yadavi M, Badiei A, Mohammadi ziarani G, Abbasi A (2013) Synthesis of novel fluorene functionalized nanoporous silica and their luminescence behavior in acid media. Chem Papers 67:751–758
21. Dong Z, Dong Z, Wang P, Tian X, Geng H, Li R, Ma J (2010) A fluorescent probe for zinc detection based on organically functionalized SBA-15. Appl Surf Sci 257:802–806
22. Chen X, Yamaguchi A, Namekawa M, Kamijo T, Teramae N, Tong A (2011) Functionalization of mesoporous silica membrane with a Schiff base fluorophore for Cu(II) ion sensing. Anal Chim Acta 696:94–100
23. Wang J, Chu S, Kong F, Luo L, Wang Y, Zou Z (2010) Designing a smart fluorescence chemosensor within the tailored channel of mesoporous material for sensitively monitoring toxic heavy metal ions Pb(II). Sens Actuators B 150:25–35
24. Metivier R, Leray I, Lebeau B, Valeur B (2005) A mesoporous silica functionalized by a covalently bound calixarene-based fluoroionophore for selective optical sensing of mercury(II) in water. J Mater Chem 15:2965–2973
25. Wlf A, Dd P (1996) Purification of laboratory chemicals. Elsevier, Burlington
26. Badiei A, Goldooz H, Mohammadi ziarani G (2011) A novel method for preparation of 8-hydroxyquinoline functionalized mesoporous silica: Aluminum complexes and photoluminescence studies. Appl Surf Sci 257:4912–4918
27. Khaniani Y, Badiei A, Mohammadi ziarani G (2012) Application of clickable nanoporous silica surface for immobilization of ionic liquids. J Mater Res 27:932–938
28. Lj J, Luo Q, Cy D, Shen Mc H, Hw LY (1999) A new dioxotetraamine ligand appended with fluorenyl and its copper(II) complex. Synthesis, crystal structure and solution behavior. Inorg Chim Acta 295:48–55
29. Socrates G (2004) Infraredand raman characteristic group frequencies. John Wiley
30. Cp J, Kruk M, Jaroniec M, Sayari A (1998) Tailoring surface and structural properties of MCM-41 silicas by bonding organosilanes. J Phys Chem B 102:5503–5510
31. Lt Z (2000) Metal—solvent interaction at electrode/solution interfaces reactivity scale in different solvents and photoemission threshold. Colloids Surf 1:173–189
32. Jl B, Ferrer R, Guiteran J (1998) Multivariate calibration of polycyclic aromatic hydrocarbon mixtures from excitation-emission fluorescence spectra. Anal Chim Acta 373:311–319
33. S.Vogt B, Schulman Sg (1982) Anomalous flourescence of 9-aminofluorene. Chem Phys Lett 89:320–23
34. Rd S (1976) Revised effective ionic radii and systematic studies of interatomic distances in halides and chalcogenides. Acta Crystallogr 32:751–767
35. Lakowicz J (1999) Principles of fluorescence spectroscopy. Kluwer Academic, Plenum Publishers, New York
36. Jw D, Yao K, Wy H, Sp B (2006) Study on the interaction of copper–zinc superoxide dismutase with aluminum ions by electrochemical and fluorescent method. Spectrochim Acta A 65:896–900
37. Mdpd C, Wapa J (2004) Detailed studies on complexation behaviour and mechanism of fluorescence quenching of naphthalene linked hydroxamic acid with transition metal ions by UV-visible and fluorescence spectra. J Photoch Photobio A 162:591–598